TEX$_{86}$ AND U$_{37}^{k\prime}$ APPLICATIONS TO AMPLIFY INFORMATION ON WESTERN BOUNDARY CURRENTS DURING THE MID- TO LATE MIOCENE

An Undergraduate Research Scholars Thesis

by

KIMBERLY SAYPRASITH

Submitted to the Undergraduate Research Scholars program at
Texas A&M University
in partial fulfillment of the requirements for the designation as an

UNDERGRADUATE RESEARCH SCHOLAR

Approved by Research Advisor: Dr. Yige Zhang

May 2020

Major: Environmental Geoscience

TABLE OF CONTENTS

ABSTRACT

TEX$_{86}$ and U$_{37}^{k'}$ Applications to Amplify Information on Western Boundary Currents during the Mid- to Late Miocene

Kimberly Sayprasith
Department of Geosciences
Texas A&M University

Research Advisor: Dr. Yige Zhang
Department of Oceanography
Texas A&M University

The Middle Miocene Climatic Optimum (MMCO) is a time period that demonstrated significantly high temperatures, which interrupted the mid-Cenozoic cooling trend. While there is abundant data on deep ocean temperatures during this mid-late Miocene, there is a lack of information on sea surface temperatures (SSTs) in the Northern Pacific Ocean and in other areas of the world. Additionally, climate models based on various CO$_2$ concentrations underestimate mean annual temperature values suggested by proxy records. Thus, more SST data must be gathered to lessen the disparity between proxy data and climate models. Additionally, SSTs can be a useful tool to track the subtropical gyre pattern during the mid- to late Miocene, which plays a pivotal role in the carbon cycle and global heat distribution. An important part of the North Pacific gyre system is the western boundary current, an area where carbon, water, and heat exchanges with the atmosphere are concentrated. Therefore, the proposed research would employ TEX$_{86}$ and U$_{37}^{k'}$ proxies to reconstruct continuous SST records from core sites around the North Pacific western boundary current, specifically the Kuroshio Current, in the mid- to late Miocene to further knowledge of ocean circulation and currents and its effects on past climate.

ACKNOWLEDGMENTS

This research project was successful thanks to my advisor, Yige Zhang, my mentor, Noura Randle, and the wonderful members in the Zhang laboratory: Bumsoo Kim, Daianne Höfig, Ronnakrit Rattanasri-ampaipong, Yang Zhang, and Xiaoqing Liu.

Many thanks towards the LAUNCH program at Texas A&M University to make this opportunity tangible and my experience at this university to be worthwhile and substantial. I also appreciate the services of the International Ocean Discovery Program for their services and cores that allow me to gather samples.

Finally, I have my utmost gratitude to my parents for their unconditional love and support throughout my college career and more.

NOMENCLATURE

ASE   Accelerated Solvent Extractor

APCI   Atmospheric pressure chemical ionization

BIT   Branched and Isoprenoid Tetraether

DSDP   Deep Sea Drilling Project

GC   Gas chromatography

GDGT   Glycerol dialkyl glycerol tetraethers

FID   Flame ionization detection

IODP   International Ocean Discovery Program

KC   Kuroshio Current

LC   Liquid chromatography

Ma   Mega- annum

mbsf   Meters below sea floor

MMCO   Middle Miocene Climatic Optimum

MS   Mass spectrometer

ODP   Ocean Drilling Program

SST   Sea surface temperature

TEX   TetraEther indeX

TLE   Total lipid extract

WBC   Western boundary current

CHAPTER I

INTRODUCTION

Since the beginning of the Cenozoic Era (65 Ma), Earth demonstrated a cooling trend. The Middle Miocene Climate Optimum (MMCO) (17-14.75 Ma) disrupted this pattern with significantly high temperatures recorded by $\delta^{18}O$ in benthic foraminiferal calcite records. According to Zachos et al. (2008), MMCO temperatures were estimated to be 5 - 6°C warmer than modern deep water temperatures. Although many proxies indicate a warming period, there are unclear reasons for the occurrence. Though greenhouse forcing has been considered a likely trigger for these warmer temperatures, reconstructed CO_2 values do not support this. Rather, CO_2 reconstructions yield values comparative to modern data ranging from 400-500 ppm based on stomatal leaf studies (Kürschner et al., 2008), boron isotopes (Foster et al., 2012), and alkenone biomarkers (Zhang et al., 2013). In addition, tectonic movement resulting in ocean gateway changes (Sloan et al., 1995) and updated atmosphere-ocean modelling (Huber and Sloan, 2001) reveal that global warming mechanisms remain inconclusive. Limited spatial and temporal proxy data constricts boundary conditions for climate models, thus overestimating the temperature gradient from the equator to the poles and underestimating mean annual temperatures (Goldner et al., 2014).

To lessen the gap between proxy records and climate models, the Pacific Ocean will be examined as it largely impacts the climate from the water, heat, and carbon exchanges with the atmosphere. The subtropical gyre plays a pivotal role in these exchanges. Circulation patterns from the middle to late Miocene can be evaluated by reconstructing sea surface temperatures (SST) provided by paleotemperature proxies. Specific focus was placed on the dynamic region in

the Northwest Pacific influenced by the Kuroshio Current (KC), a western boundary current (WBC). These types of investigations are important to understand how geosystems change and its contributed effect on climate. This will allow a better understanding of the ocean circulation in the Miocene epoch, which serves the purpose of this research.

Western Boundary Currents

The climate is heavily influenced by the ocean's physical, chemical, and biological properties. Ocean circulation transports heat from the tropics to high latitudes and from the ocean to the atmosphere globally. This process is concentrated along western boundary currents between 25° and 45° N. As WBC transport warm tropical water pole wards, heat and humidity are transferred to the atmosphere. As water vapor cools, gas solubility increases and CO_2 from the atmosphere is absorbed by these surface waters. There are western boundary currents in the southern hemisphere, although they are not as strong compared to the northern hemisphere due to continental configuration. Specifically, the Kuroshio Current (KC) in the Pacific Ocean and the Gulf Stream in the North Atlantic deliver 70% of ocean heat to the atmosphere (Kwon et al., 2010). The KC will be examined further by collecting SST data from the middle to late Miocene epoch through studying sites surrounding Japan. The KC splits around Japan, divided into the east and west coast, thus sites are chosen from both sides (Fig. 1).

Sites

The western coast covers Ocean Drilling Program (ODP) Leg 127 and sites 795 and 797, which are found in the northern Japan Basin and southern Yamato Basin, respectively. The KC predominantly flows on the eastern coast. ODP Leg 186-1151 and Deep Sea Drilling Project (DSDP) Leg 57-438 are sites west of Japan Trench. All four sites have a considerable concentration of nannofossils and moderate to high sedimentation rate in the middle to late Miocene. Sediment samples rich with organic material are likely to have biomarkers present.

Modern temperature on the sites were evaluated on Ocean Data View software using data from Locarnini et al. (2013) and shown in Fig. 1 with the modern site locations. Latitudinal gradient was measured by comparing sites 795 and 797, likewise with 438 and 1151. The difference in mean annual temperatures between sites 795 and 797 was 5.21°C. The difference between sites 438 and 1151 was 3.36°C. Additionally, a comparison was made with the east and west coast of Japan. Sites 795 and 438 was compared, as well as 797 with 1151. Both comparisons revealed to be about a degree difference. Based on the latitudinal gradient, the western coast has a larger temperature difference. This suggests that the KC has a reduced influence as it reaches 795, causing the temperatures to be cooler than its counterpart site 438. Its higher latitudinal location contributes to its cooler temperature as well.
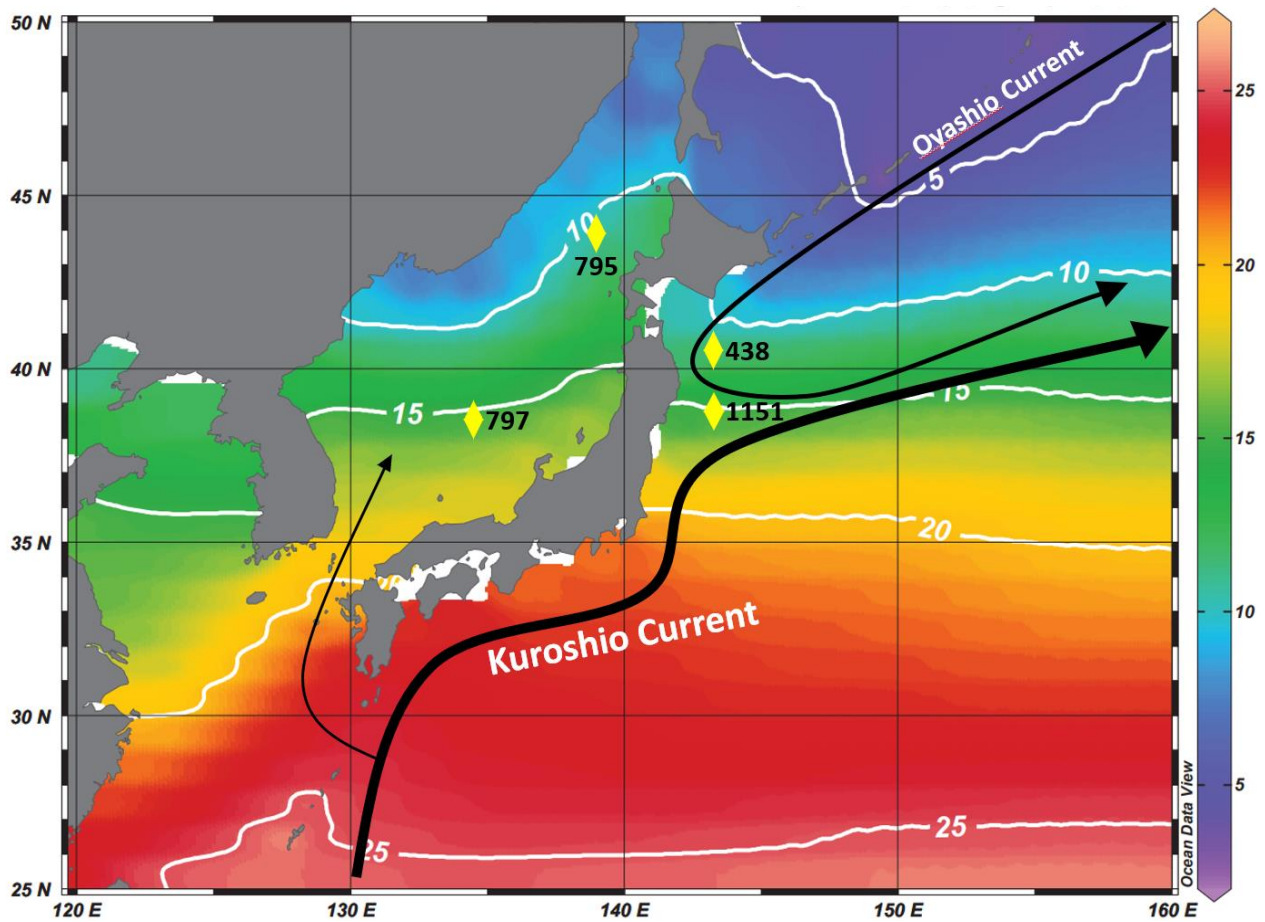

Figure 1. Modern sites with the KC

Paleotemperature Proxies

Alkenone based $U_{37}^{k\prime}$ temperature proxy

Alkenones originate from haptophyte algae that reside in the upper photic zone (Popp et al., 2006). The alkenone method proves to be advantageous to use compared to other proxies. The GC analyzes a higher volume of data faster and produces high signal-noise ratios. Moreover, the alkenones remain persistent to diagenesis. However, haptophyte algae population changes volume seasonally and do not remain at the same depth in the water column (Herbert, 2014), although still limited to remaining within the photic zone and therefore staying near surface. Nevertheless, the alkenone method demonstrates a promising relationship with SST depending on di- and tri- unsaturated ketones proportions to find the $U_{37}^{k\prime}$ index, defined in $U_{37}^{k\prime} = C_{37:2}/(C_{37:2} + C_{37:3})$ ($C_{37:2}$ = diunsaturated ketone; $C_{37:3}$ = triunsaturated ketone) (Prahl and Wakeham, 1987). According to Conte et al. (2006), $r^2 = 0.97$ shows a strong relationship supported by core top calibrations. Temperature is calibrated using equations given by Conte et al. (2006).

GDGT based TEX_{86} temperature proxy

TetraEther indeX (TEX) of 86 carbon atoms come from the relative composition of crenarchaeotal glycerol dialkyl glycerol tetraethers (GDGT) lipids influenced by temperature (Schouten et al., 2013). GDGTs show to be recalcitrant to diagenesis and are capable of displaying higher growth temperatures compared to $U_{37}^{k\prime}$, which has an upper limit of 28.5°C. Although, given the northern location of the sites and time period, it would be unlikely for reconstructed temperatures to exceed 28.5°C. Despite these advantages, TEX_{86} values can be uncertain due to varying depth and seasonality of GDGT population. In order to test the reliability of TEX_{86} data, multiple proxies have been developed to ensure data affected by non-thermal factors are not used. The Ring Index uses the weight of cyclopentane moieties to

ascertain if TEX_{86} SST estimates derive from thermal influences (Zhang et al., 2016). The

Methane Index depends on the signal from methanotrophic archaeal species based on GDGT -1,

-2, -3 to determine if TEX_{86} temperature reconstructions are robust (Zhang et al., 2011). The

Branched and Tetraether Index (BIT) differentiate between GDGT and crenarchaeol abundances

to analyze the influences from terrestrial environments (Hopmans et al., 2004).

Different types of GDGTs contain 0-3 cyclopentanes (GDGT 0-3), crenarchaeol (GDGT

4), and regioisomer of crenarchaeol (GDGT 4'). The GDGT assortment constitute the TEX_{86}

index in $TEX_{86} = ([2] + [3] + [4'])/([1] + [2] + [3] + [4'])$ (Schouten et al., 2007). TEX_{86} values

were converted to SST estimates using the high temperature calibrations from (Kim et al., 2010),

in addition to the multiple quality control proxies mentioned above to screen the data.

CHAPTER II

METHODS

Sample Preparation

Sediment samples were acquired from International Ocean Drilling Program (IODP) and then freeze dried to eliminate moisture. 20 to 40 g of bulk sediment were ground and homogenized using an ashed mortar and pestle. Aliquots of each sample were loaded onto Accelerated Solvent Extractor (ASE) cells. Total lipid extracts (TLEs) were obtained using DIONEX^{TM} ASE under 120°C and 7.6 X 10^6 Pa using a mixture of dichloromethane (DCM):methanol (MeOH) (9:1, vol/vol). TLEs were dried down and concentrated under a stream of ultra- pure N$_2$ gas.

Two methods of sample preparation were employed to analyze GDGTs and alkenones: TLE filtering and silica gel chromatography. A TLE screening was performed on a subset of samples from each site to identify their viability for GDGT and alkenone analysis. All sites exhibited promise for GDGTs, while only site 438 suggested the presence of alkenones in measurable quantities. Samples from sites 795, 797, and 1151 were reconstituted in hexane:isopropanol (99:1, v/v), then strained using 2 μm ashed glass filter. Samples from 438 were further processed by using silica gel chromatography, wherein the TLEs were separated into aliphatic, aromatic, and polar fractions from the elution of hexane, DCM, and MeOH, respectively. The aromatic (DCM) fraction contained the alkenones and the polar fraction (MeOH) contained the GDGTs. These sample preparation methods follow those described in Zhang et al. (2013).

9

Sample Analysis

GDGTs

Samples eluted by MeOH or TLE filtered containing GDGTs were analyzed using an Agilent 1260 high-performance liquid chromatography/ atmospheric pressure chemical ionization mass spectrometer (HPLC/ APCI-MS). GDGTs were separated using two solvents with the Acquity UPLC Glycan BEH amide columns in tandem at 50°C. Solvent A was hexane and solvent B was a mixture of hexane:isopropanol (99:1, v/v). Initially, 97% of A and 3% of B flowed through the columns at 0.40 mL min^{-1}. After 35 minutes, the ratio changed to 50% of A and B. At 45 minutes, the columns are flushed with a 100% of B. The Agilent 6120 Quadruple LC/MS identified compounds and relative abundance using a selected ion monitoring mode, for the specific *m/z* ratios of the GDGT compounds of interest. The sample analysis methodology was listed in Becker et al. (2013) and Zhang et al. (2013). Using peak integration to quantify relative abundance of GDGTs, TEX$_{86}$ was calculated to reconstruct SSTs. Various temperature calibrations (Kim et al., 2010; Tierney and Tingley, 2015) was applied to fit the dataset appropriately.

Alkenones

The DCM fraction containing alkenones used an Agilent 7890B Gas Chromatography with Flame Ionization Detection (GC-FID) for alkenone separation and compound identification. Helium acted as a carrier gas through the Agilent 122-1062 column. The oven was held at 70°C for 2.50 minutes, then eventually heated to 320°C. Alkenone compounds were determined by the elution times in comparison with standards that was run for every five samples. These methods were adapted from Herbert et al. (2016). Di- and tri- unsaturated ketone abundances are used to

calculate $U_{37}^{k'}$ to estimate past SSTs. Temperature measurements were refined using equations given by Conte et al. (2006).

Age Models

   Age models for each site were developed from updated magnetostratigraphy and biostratigraphy datums from DSDP and ODP Initial Reports and Scientific Findings and Geologic Times Scale 2012 (Gradstein et al., 2012). Specific sample age models were developed from using the interpolation command in MATLAB. Magnetostratigraphy and biostratigraphy are methods that aided in evaluating approximate age datums. Magnetostratigraphy is a powerful tool that bases on the pole reversals in the Earth's magnetic field and the magnetic imprint in sediments. It provides a more accurate dating than biostratigraphy, a method that relies on the appearance and disappearance of planktonic microfossils. However, the methods combined makes the age model a more precise representation. Table 1 (below) shows the interpolated ages with corresponding sediment depth for each sample including the dataset from Wittkopp et al. (2017) highlighted in green.

Table 1. Age model of sites. Wittkopp et al. (2017) is depicted in green.

1151A		795B		797B		438A	
mbsf	Age (Ma)	mbsf	Age (Ma)	mbsf	Age (Ma)	mbsf	Age (Ma)
296.2	4.52733	325.57	5.81072	243.54	7.6954	328.11	5.00417
377.03	4.64655	365.74	6.83053	250.28	7.75889	395.05	6.00219
454.64	4.7578	395.42	7.58404	274.755	8.24796	448.57	7.00645
541.22	4.93611	433.225	8.80946	278.61	8.38923	625.16	9.77986
623.09	5.47114	466.67	9.69461	299.46	9.17225	650.9	11.2395
704.455	6.11252	519.83	10.8384	300.38	9.20737	662.99	12.0011
786.2	6.55738	540.3	11.2222	303.84	9.33947	680.93	12.9205
867.44	7.82298	577.73	11.8364	319.07	9.92091	703.36	14.0037
947.71	9.02436	616.23	12.4683	321.12	9.99917	718.81	14.4879
1037.07	14.0229			340.81	10.7509	721.57	14.524
1068.67	14.7994			351.02	11.1407	725.18	14.5668
1073.62	14.9165			359.92	11.4804	726.77	14.5841
1077.15	14.9999			369.595	11.8498	729.27	14.6098
1078.29	15.0269			380.54	12.0594	731.78	14.6336
1084.67	15.1913			397.71	12.388	733.15	14.6458
1096.99	15.706			417.11	12.7593	736.49	14.6734
1104.05	16.0001			426.79	12.9445	738.985	14.6921
1108.49	16.1841			437.34	13.1464	741.63	14.7105
1112.36	16.3444			437.96	13.1583	745.33	14.7337
				439.95	13.1964	746.7	14.7417
				442.49	13.245		
				447.62	13.3432		
				447.73	13.3453		
				449.91	13.4866		
				452.86	13.7515		
				458.71	14.2769		
				459.87	14.381		
				462.2	14.5903		
				462.275	14.597		
				463.29	14.6882		
				475.175	15.7555		
				479.1	16.1079		
				484.56	16.5983		
				485.61	16.6925		
				493.92	17.4388		

CHAPTER III

RESULTS

Most of the samples were similar to Fig. 3, thus only TEX86 was calculated for temperature reconstructions. In addition to the site 797, another subset of samples from Wittkopp et al. (2017) were used for a more accurate representation of temperature trends. Although there were samples from 438 that showed promise for alkenone temperature reconstructions, when run on the GC-FID the peaks of interest overlapped and therefore it was not possible to calculate the $U_{37}^{k\prime}$ ratio with confidence without further sample preparation. Additional published data for site 797 was available from Wittkopp et al. (2017) allowed for increased sample resolution at this site.
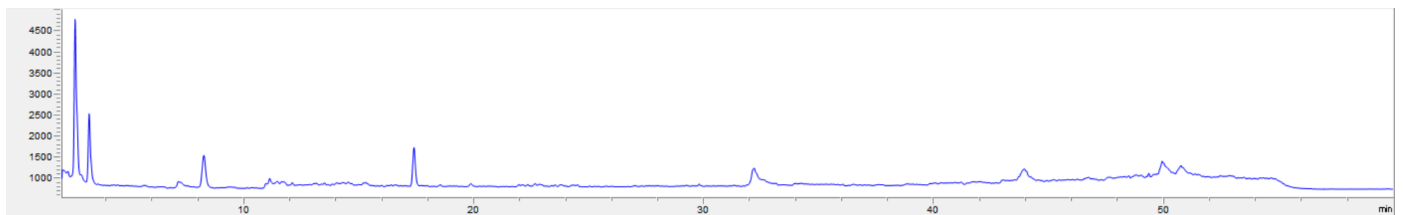

Figure 2. Environmental standard sample with presence of alkenones in the first few minutes.
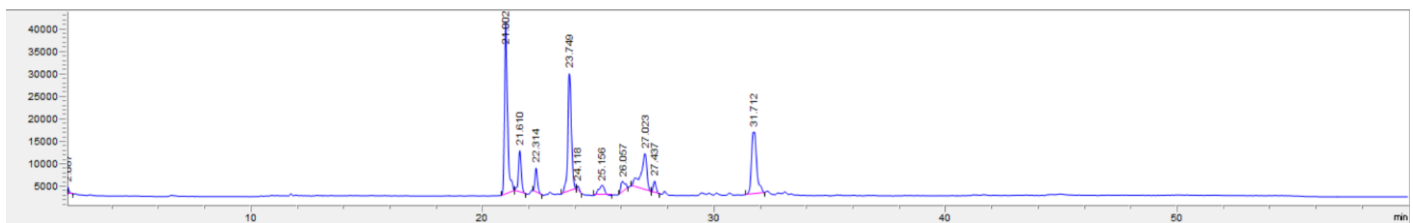

Figure 3. Environmental standard sample with presence of GDGTs. The first four peaks are measured.

Calculated SSTs for each site are seen below in Figure 4, below. As expected, all sites demonstrate a cooling trend after the MMCO. During the optimum, sites 438, 1151, and 797 do not show a significant temperature difference. Afterwards in the transition phase, a temperature gradient is amplified between the sites. 797 exhibits high amplitude changes in this data and Wittkopp's data, which suggests climate instability. A warming is depicted around 8-9 Ma, then a steep cooling in sites 795, 797, and 1151. A mean gradient was calculated between sites 795 and 797, resulting in a 4.28°C, which was a degree difference from the modern gradient. Between sites 438 and 1151, there was a smaller magnitude of 1.28°C compared to present temperature differences and smaller than the calibration uncertainty of the TEX86 proxy. Longitudinal temperature differences were measured, which revealed northern sites with a 1.05°C difference and southern sites to be a 1.95°C difference. In the late Miocene around 7 Ma, 1151 has a delayed cooling compared to its western counterpart. Furthermore, 795 appears to be the earliest site to start cooling in the late Miocene.
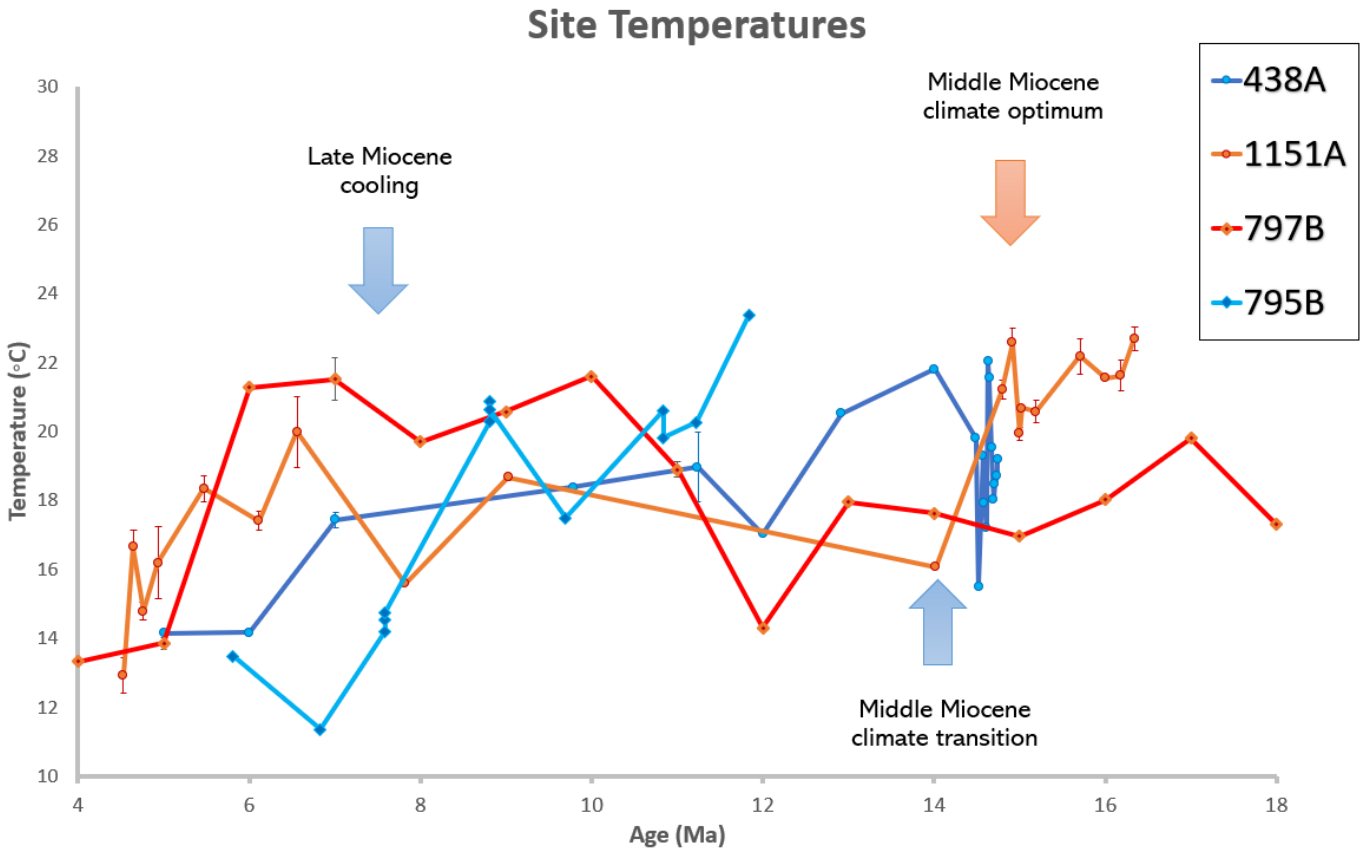
Figure 4. Site temperatures with additional data from Wittkopp et al. (2017) over the last 18 million years.

CHAPTER IV

CONCLUSION

Resulting temperature trends prove similar to other published papers like Herbert et al. (2016), Zachos et al. (2008), and Zhang et al. (2013). A cooling trend is expected after the climatic optimum to continue the glaciation process, although site 797 depicts evidence of climate instability following the MMCT with rapid and high amplitude SST changes. During the transition, a small temperature gradient may be from shifted ocean gateways in tectonic movement that impacted the distribution of KC flow on the western and eastern coast, however further research that is beyond the scope of this project would be required. In addition, the cooling acceleration may have resulted from a positive feedback loop from the initial cooling of the ocean through the decline of CO_2 and atmospheric water vapor.

Latitudinal Analysis

Based on the mean temperature of the sites in the Japan Sea, it is possible the KC affected site 795 more by its stronger water flow into the coast. The lack of a gradient during the MMCO suggests the KC may have intruded further north before breaking off from the Japan coast. The gradient that develops in the late Miocene may be a result of the KC shifting to a position similar to modern day. Furthermore, when 795 has an accelerated cooling than other sites, this suggests a weakening influence from the KC in the northern part of the Japan Sea. On the eastern coast of Japan, a smaller gradient between sites 438 and 1151 is identified. This may be due to the extension occurring just north of 438.

Longitudinal Analysis

There is a similar temperature difference in the northern sites compared to modern temperatures, possibly from an equal discharge from the KC. On the southern counterpart, the delayed cooling from site 1151 may result from a slow eastward shift of the KC.

Future Progression

A clearer understanding of the KC shift in circulation can be done from increasing sample resolution from each site and investigating additional sites around Japan. A closer overview of tectonic movement and shifted ocean gateways can be examined closer to narrate the movement of the KC.

In the hopes of supplying temperature reconstructions to a western boundary current that significantly affects the climate, climate models can evaluate the progression of Earth's climate more clearly. More importantly, when the increased challenges of anthropogenic climate change can blur climate forecast, an understanding of past ocean circulation and biogeochemical cycles can provide insight of the future.

REFERENCES

Becker, K. W., Lipp, J. S., Zhu, C., Liu, X.-L., & Hinrichs, K.-U. (2013). An improved method for the analysis of archaeal and bacterial ether core lipids. *Organic Geochemistry*, *61*, 34–44. https://doi.org/10.1016/j.orggeochem.2013.05.007

Foster, GL et al. (2012): The evolution of pCO2, ice volume and climate during the middle Miocene. *Earth and Planetary Science Letters*, 341-344, 243-254, https://doi.org/10.1016/j.epsl.2012.06.007

Goldner, A., Herold, N., & Huber, M. (2014). The challenge of simulating the warmth of the mid-Miocene climatic optimum in CESM1. *Climate of the Past*, *10*(2), 523–536. https://doi.org/10.5194/cp-10-523-2014

Gradstein, F. M., Ogg, J. G., Schmitz, M. D., & Ogg, G. M. (Eds.). (2012). Copyright. In *The Geologic Time Scale* (p. iv). Elsevier. https://doi.org/10.1016/B978-0-444-59425-9.02002-3

Herbert, T. D. (2014). Alkenone Paleotemperature Determinations. In *Treatise on Geochemistry* (pp. 399–433). https://doi.org/10.1016/B978-0-08-095975-7.00615-X

Herbert, T. D., Lawrence, K. T., Tzanova, A., Peterson, L. C., Caballero-Gill, R., & Kelly, C. S. (2016). Late Miocene global cooling and the rise of modern ecosystems. *Nature Geoscience*, *9*(11), 843–847. https://doi.org/10.1038/ngeo2813

Hopmans, Ellen & Weijers, Johan & Schefuß, Enno & Herfort, Lydie & Sinninghe-Damste, J. & Schouten, Stefan. (2004). A novel proxy for terrestrial organic matter in sediments based on branched and isoprenoid tetraether lipids. *Earth and Planetary Science Letters.* 224. 107-116. https://doi.org/10.1016/j.epsl.2004.05.012

Huber, M., and L. C. Sloan, 2001: Heat transport, deep waters, and thermal gradients: Coupled simulation of an Eocene greenhouse climate. *Geophysical Research Letters*, 28, 3481-3484.

Kim, J.-H., van der Meer, J., Schouten, S., Helmke, P., Willmott, V., Sangiorgi, F., Koç, N., Hopmans, E. C., and Damsté, J. S. S., 2010, New indices and calibrations derived from the distribution of crenarchaeal isoprenoid tetraether lipids: Implications for past sea surface temperature reconstructions. *Geochimica et Cosmochimica Acta*, v. 74, p. 4639-4654.

Kurschner, W. M., Kvacek, Z., & Dilcher, D. L. (2008). The impact of Miocene atmospheric carbon dioxide fluctuations on climate and the evolution of terrestrial ecosystems. *Proceedings of the National Academy of Sciences*, *105*(2), 449–453. https://doi.org/10.1073/pnas.0708588105

Kwon, Y.-O., Alexander, M. A., Bond, N. A., Frankignoul, C., Nakamura, H., Qiu, B., & Thompson, L. A. (2010). Role of the Gulf Stream and Kuroshio–Oyashio Systems in Large-Scale Atmosphere–Ocean Interaction: A Review. *Journal of Climate*, *23*(12), 3249–3281. https://doi.org/10.1175/2010JCLI3343.1

Locarnini, R. A., A. V. Mishonov, J. I. Antonov, T. P. Boyer, H. E. Garcia, O. K. Baranova, M. M. Zweng, C. R. Paver, J. R. Reagan, D. R. Johnson, M. Hamilton, and D. Seidov (2013). *World Ocean Atlas 2013, Volume 1: Temperature.* S. Levitus, Ed., A. Mishonov Technical Ed.; NOAA Atlas NESDIS 73, 40 pp.

Lyle, M., Barron, J., Bralower, T. J., Huber, M., Olivarez Lyle, A., Ravelo, A. C., Rea, D. K., & Wilson, P. A. (2008). Pacific Ocean and Cenozoic evolution of climate. *Reviews of Geophysics*, *46*(2), RG2002. https://doi.org/10.1029/2005RG000190

Popp, B. N., Prahl, F. G., Wallsgrove, R. J., & Tanimoto, J. (2006). *Seasonal patterns of alkenone production in the subtropical oligotrophic North Pacific*. *21*(1). https://doi.org/10.1029/2005PA001165

Prahl, F. G., and S. G. Wakeham (1987), Calibration of unsaturation patterns in long-chain ketone compositions for paleotemperature assessment. *Nature*, 330(6146), 367–369, doi:10.1038/330367a0.

Schouten, S., Forster, A., Panoto, F. E., & Sinninghe Damsté, J. S. (2007). Towards calibration of the TEX86 palaeothermometer for tropical sea surface temperatures in ancient greenhouse worlds. *Organic Geochemistry*, *38*(9), 1537–1546. https://doi.org/10.1016/j.orggeochem.2007.05.014

Schouten, S., Hopmans, E. C., & Sinninghe Damsté, J. S. (2013). The organic geochemistry of glycerol dialkyl glycerol tetraether lipids: A review. *Organic Geochemistry*, *54*, 19–61. https://doi.org/10.1016/j.orggeochem.2012.09.006

Sloan, L. C., J. C. G. Walker, and T. C. Moore Jr, 1995: Possible role of oceanic heat transport in early Eocene climate. *Paleoceanography*, 10, 347-356

Tierney, J. E., & Tingley, M. P. (2015). A TEX$_{86}$ surface sediment database and extended Bayesian calibration. *Scientific data*, *2*, 150029. https://doi.org/10.1038/sdata.2015.29

Wittkopp, Frederike; Yamamoto, Masanobu; Moossen, Heiko; Dunkley Jones, Tom; Henderson, Andrew C G H; Bendle, James A (2017): Sea surface temperature estimates for sediment cores in the Japan Sea. PANGAEA, https://doi.org/10.1594/PANGAEA.879742

Zachos, J. C., Dickens, G. R., & Zeebe, R. E. (2008). An early Cenozoic perspective on greenhouse warming and carbon-cycle dynamics. *Nature*, *451*(7176), 279–283. https://doi.org/10.1038/nature06588

Zhang, Y. G., Zhang, C. L., Liu, X.-L., Li, L., Hinrichs, K.-U., & Noakes, J. E. (2011). Methane Index: A tetraether archaeal lipid biomarker indicator for detecting the instability of marine gas hydrates. *Earth and Planetary Science Letters*, *307*(3–4), 525–534. https://doi.org/10.1016/j.epsl.2011.05.031

Zhang, Y. G., Pagani, M., Liu, Z., Bohaty, S. M., & DeConto, R. (2013). A 40-million-year history of atmospheric CO $_2$. *Philosophical Transactions of the Royal Society A: Mathematical, Physical and Engineering Sciences*, *371*(2001), 20130096. https://doi.org/10.1098/rsta.2013.0096

Zhang, Y. G., Pagani, M., & Wang, Z. (2016). Ring Index: A new strategy to evaluate the integrity of TEX_{86} paleothermometry: Quality Control For Tex_{86} Temperatures. *Paleoceanography*, *31*(2), 220–232. https://doi.org/10.1002/2015PA002848